A Highly Water Stable *meta*-carborane based Copper-Metal-Organic Framework for Efficient High-Temperature Butanol Separation

Lei Gan,[a] Arunraj Chidambaram,[b] Pol G. Fonquernie,[a] Mark E. Light,[c] Duane Choquesillo-Lazarte,[d] Hongliang Huang,[e] Eduardo Solano,[f] Julio Fraile,[a] Clara Viñas,[a] Francesc Teixidor,[a] Jorge A. R. Navarro,[g] Kyriakos C. Stylianou,* [b,h] José G. Planas*[a]

[a] Institut de Ciència de Materials de Barcelona (ICMAB-CSIC)
Bellaterra, Spain.

E-mail: jginerplanas@icmab.es

[b] Institute of Chemical Sciences and Engineering, École Polytechnique Fedérale de Lausanne (EPFL Valais), Rue de l'Industrie 17, 1951 Sion, Switzerland.

[c] Department of Chemistry, University of Southampton, Highfield, Southampton SO17 1BJ, UK.

[d] Laboratorio de Estudios Cristalográficos, IACT, CSIC-Universidad de Granada, Av. de las Palmeras 4, E-18100 Armilla, Granada, Spain.

[e] State Key Laboratory of Separation Membranes and Membrane Processes, School of Chemistry and Chemical Engineering, Tiangong University, Tianjin 300387, China.

[f] NCD-SWEET beamline, ALBA Synchrotron Light Source, 08290 Cerdanyola del Vallès, Barcelona, Spain.

[g] Departamento de Química Inorgánica, Universidad de Granada, Av. Fuentenueva S/N, E-18071, Granada, Spain.

[h] Department of Chemistry, Oregon State University, 153 Gilbert Hall, OR 97331, Corvallis, Oregon, USA.

E-mail: kyriakos.stylianou@oregonstate.edu

Keywords: Metal-organic frameworks, hydrophobicity, carborane, butanol recovery, water stability

Abstract: Biofuels are considered a sustainable and renewable alternative to conventional fossil fuels. Biobutanol has recently emerged as an attractive option compared to bioethanol and biodiesel, but a significant challenge in its production lies on the separation stage. The current industrial process for the production of biobutanol includes the ABE (acetone-butanol-ethanol) fermentation process from biomass; the resulting fermentation broth has a butanol concentration of no more than 2 wt% (the rest is essentially water). Therefore, the development of cost-effective butanol separation processes from dilute aqueous solutions is highly desirable. The use of porous materials for the adsorptive separation of ABE mixtures is considered a highly promising route, as these materials can potentially have high affinities for alcohols and low affinities for water. To date, zeolites have been tested towards this separation, but their hydrophilic nature makes them highly incompetent for this application. The use of metal-organic frameworks (MOFs) is an apparent solution, however, their low hydrolytic stabilities hinder their implementation in this application. So far, a few nanoporous zeolitic imidazolate frameworks (ZIFs) have shown excellent potential for butanol separation due to their good hydrolytic and thermal stabilities. Herein, we present a novel, porous and hydrophobic MOF based on copper ions and carborane-carboxylate ligands, ***m*CB-MOF-1**, for butanol recovery. ***m*CB-MOF-1** exhibits excellent stability when immersed in organic solvents, water at 90 ºC for at least two months and acidic and basic aqueous solution We found that, like ZIF-8, ***m*CB-MOF-1** is non-porous to water (type II isotherm), but it has higher affinity for ethanol, butanol and acetone compared to ZIF-8 as suggested by the shape of the vapor isotherms at the crucial low-pressure region. This is reflected in the separation of a realistic ABE mixture in which ***m*CB-MOF-1** recovers butanol more efficiently compared to ZIF-8 at 333 K.

INTRODUCTION

Biofuels are gaining a continual prominence, primarily to augment the security of energy and supply, and thus contribute to the development of a sustainable economy. Biofuels are also emerging as one of the overarching solutions for Bioenergy with Carbon Capture and Storage (BECCS), a negative emission technology for meeting the global warming target.[1-2] It is therefore, not surprising that many countries promote the use of biofuels through supportive legislation, policy measures, and capital investments. For example, The Energy Policy Act (2005) directed that all fuels produced in the USA must contain a minimum volume of renewable fuels (such as biofuels). This has resulted in the commercial availability of biobutanol blended gasoline (with up to 16% biobutanol by volume).[3] The growing interest is further reflected by the annual global biofuel production figures, which shows that the year 2018 had the highest global biofuel production in recent times. The IEA forecasts this trend will rise to 25% by 2024, with the USA and Brazil accounting for two-thirds of the global production.[4]

Biobutanol is considered as an attractive renewable transportation fuel as it exhibits superior performance and properties when is compared with bioethanol.[5] Biobutanol is less hydroscopic, has higher energy density (30% on a unit volume basis, 98% of that of gasoline), lower vapor pressure, and superior miscibility with gasoline. Also, biobutanol is considered a viable biochemical alternative to synthetic butanol, whose costs are determined by crude oil prices. It can potentially replace petro-butanol, and be an essential precursor for mainstream industrial chemicals and several high-value products like paints, polymers, and plastics. Owing to the prospective multisector applications, there has been an increasing commercial interest in the production of biobutanol. Typically, biobutanol is produced through the Acetone-Butanol-Ethanol (ABE) fermentation process of biomass feedstock. The critical challenge we have to overcome with this process lies in the low yield and productivity, with biobutanol being a dilute alcohol-in-water solution (concentration of < 2 wt%), resulting in prohibitively expensive downstream processing costs. Addressing this challenge can enhance the technical and economic viability of this process. To date, there are two proposed approaches to overcome this: i. Through genetic engineering-based modification of microorganisms to enhance the product yield and concentration and thereby reducing the production costs and ii. Through the development of a downstream (hybrid) separation process, which is cost-effective, energy-efficient, and easily integrated with the ABE fermentation reactor in recovering biobutanol.[6-8]

The traditional distillation process is identified as the most energy demanding separation technique for the recovery of biobutanol owing to the evaporation of high-water content (>95%) in the feed stream. Additionally, through distillation, azeotropes might be formed. Alternatively, several prospective technologies have been suggested to make the biobutanol recovery process profitable.[9-11] Amongst these, adsorption is identified as one of the energy-efficient alternatives.[12] Adsorbent materials such as polymeric resins, activated carbon, zeolites, zeolitic imidazolate frameworks (ZIFs) and metal-organic frameworks (MOFs) have been tested towards biobutanol recovery, and most studies reported in the literature are performed predominantly under liquid-phase conditions.[13] On the other hand, the gas stripping separation technique functions by the selective removal of volatile products, i.e., ABE from the fermentation broth, which is later condensed to yield biobutanol.[14] This stripping is performed with the aid of a sparging gas like N_2, CO_2 or He. Gas stripping facilitates a higher recovery of ABE in the vapor phase than in the liquid phase. In addition, unlike liquid phase sorption, gas stripping ensures the circumvention of non-volatiles like microbial cells, sugars, and/or reaction intermediates (acetic acid and butyric acid) being removed from broth. However, it suffers from low selectivity and the possibility to form foams within the fermenter.

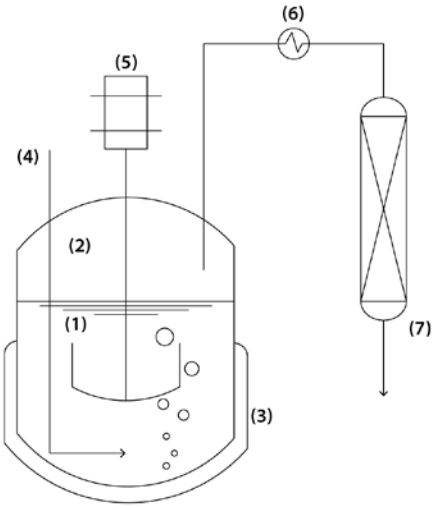

Figure 1. Schematic illustration of the integrated gas stripping and vapor phase adsorption and separation of butanol from the ABE fermentation process. (1) The ABE fermentation broth, (2) headspace of the bioreactor where ABE vapors are accumulated due to (3) heating jacket which maintains the broth at 313 K, (4) N_2 stripping gas and (5) agitator facilitate the stripping of ABE in their vapor phase as a dilute stream from the broth (6) which is heated to 333 K and (7) transferred as the feed stream to the adsorption column packed with ***m*CB-MOF-1**.

A hybrid separation technique that combines the merits of gas stripping and vapor phase adsorption and effectively overcomes the demerits of their standalone processes was recently proposed.[15-16] It involves the removal of acetone, butanol, and ethanol in their vapor state from liquid solutions using a sparging gas, and subsequently, through vapor adsorption, the separation of biobutanol is achieved (Figure 1). In that respect, a system that uses humid CO_2 to sparge the fermenter and ZIFs as adsorbents for biobutanol separation becomes the only MOF based system to be reported to date.[17] Overall, the critical issue that has to be addressed is the employment of a suitable adsorbent which has particular prerequisites: **i.** High hydrolytic stability and hydrophobicity with negligible water vapor uptake through the entire activity range, **ii.** High affinity for butanol vapor at low coverage and high uptake capacity, and **iii.** Ease of desorption and regeneration. Though zeolites are widely utilized for a plethora of applications, their hydrophilic nature makes them highly incompetent for this application. The applicability of the hydrophobic silicalite class of zeolites like Si-LTA, Si-CHA for biobutanol recovery in a gas stripping-adsorption system was recently demonstrated[18] and it was found that the selectivity of Si-LTA for butanol/ethanol was affected negatively; this was due to the adsorption of water molecules in the pores. Nonetheless, the separation of butanol was achieved with a reduced selectivity. This characteristic of high sensitivity to even small amounts of water is considered to originate from the hydrophilic defects in zeolites, and the transferability of such defects to bulk synthesis of silicalite zeolites is highly probable. MOFs are comparatively more promising candidates than zeolites for ABE separation as their structures can be tuned and tailor-made to be intrinsically hydrophobic through the application of diverse synthetic options and use of starting materials. Due to their designable structure and the resultant diverse chemical and physical properties, MOFs are useful for a variety of applications**.**[19-30] Hitherto, in the context of biobutanol recovery, hydrophobic zeolitic imidazolate frameworks (ZIFs), ZIF-8 and ZIF-71 were principally investigated for their adsorptive ABE separation as they have a low affinity for water compared to other hydrophilic ZIFs like ZIF-90.[31-41]

To improve the hydrolytic and thermal stability, as well as the hydrophobicity of MOFs, ligands based on carboranes can be introduced within their structures.[42-44] Icosahedral boranes and carboranes ($[B_{12}H_{12}]^{2-}$ and 1,n-$C_2B_{10}H_{12}$ (n = 2, 7 or 12) are a class of commercially available and exceptionally stable 3D-aromatic boron-rich clusters that possess material-favorable properties such as thermal and chemical stability and high hydrophobicity.[3, 45-48] The neutral carboranes are

remarkably robust boron clusters with two carbon atoms and possess 26 electrons for 12 vertices. The delocalized electron density is not uniform through the cage, giving rise to extraordinary differences in the electronic effects of the cluster.[49] This unusual electronic structure is often highlighted by regarding carboranes as inorganic three-dimensional "aromatic" analogs of arenes.[50] The spherical nature of the carboranes, with slightly polarized hydrogen atoms and the presence of the hydride-like hydrogens at the B-H vertexes, make the carboranes very hydrophobic.[3] Such properties make icosahedral carborane clusters valuable ligands for coordination polymers (CPs) or MOFs.[51-52] For example, some of us have reported that the hydrophobic properties of carboranes, exploited in a number of medical applications[3, 53-57] but underexploited in materials science, and can potentially enhance the hydrolytic stability of CPs and MOFs. We recently reported the first example of a MOF based on *o*-carborane as a ligand; we found that our 3-dimensional MOF was porous, hydrophobic and water stable.[44] This report was followed by a series of *m*-carborane based Co and Zn coordination polymers with high hydrolytic stabilities.[42-43]

Inspired by the intriguing properties of carborane based MOFs, herein, we report a novel Cu_2-paddlewheel based MOF with formula $[Cu_2(mCB\text{-}L)_2(DABCO)_{0.5}(H_2O)]$ (***m*CB-MOF-1**; mCB-L: 1,7-di(4-carboxyphenyl)-1,7-dicarba-closo-dodecaborane; DABCO: 1,4-diazabicyclo[2.2.2]octane; Figure 2) for butanol recovery. Our porous and hydrophobic ***m*CB-MOF-1** retains its porosity when subjected to harsh aqueous conditions (e.g., pH 2-11 for one day or at 90 ºC for over two months). Owing to the excellent hydrolytic stability of ***m*CB-MOF-1**, it was tested as an absorbent for ABE separation and compared with ZIF-8. Unlike ZIF-8, the S-shaped alcohol and acetone isotherms with low pressure uptakes are not observed for ***m*CB-MOF-1**, indicating a stronger interaction between the adsorbate and adsorbent. The performance of ***m*CB-MOF-1** towards ABE separation was evaluated in vapor phase dynamic adsorption breakthrough experiments and showed that ***m*CB-MOF-1** is a superior adsorbent for the separation of biobutanol compared to ZIF-8 at 333 K.

RESULTS AND DISCUSSION

Crystal structure and characterization. Reaction of $Cu(NO_3)_2$ with *m*CB-H_2L and DABCO in a mixture of dimethylformamide (DMF)/ethanol/water (5:5:1) at 80 ºC for 48h afforded greenish

crystals for $[Cu_2(mCB\text{-}L)_2(DABCO)_{0.5}(H_2O)]$ (***m*CB-MOF-1**; Figure 2 and Figure S1) in 50% yield. The IR spectrum showed a characteristic broad B-H stretching band from the carborane (2601 cm^{-1}), and the C=O vibration of the carboxylate groups (1716 cm^{-1}; Figure S2). Single crystal X-ray diffraction revealed that ***m*CB-MOF-1** crystallized in the tetragonal space group *I422* and possesses a 2-fold interpenetrated 3D framework having a rare 5-connected $(4^4)(6^6)$ (Schläfli symbol) topology (Figure 2 and Table S1). Phase purity was confirmed by elemental analysis and powder X-ray diffraction (PXRD; Figure S3). The basic unit of ***m*CB-MOF-1** is a Cu_2-paddlewheel motif of $[Cu_2(COO)_4]$ units (Figure 2a). The Cu–Cu distance in the paddlewheel unit is 2.6641(5) Å. The two copper atoms share four *m*CB-L linkers at the basal positions and one oxygen atom from a water molecule and a nitrogen atom from a DABCO molecule occupy the apical positions (Figure 2a). Cu–OOC and $Cu–O_{solv}$ bond lengths range from 1.937(2) to 1.974(2) Å and 2.188(4) Å, respectively. The Cu–N bond length is 2.180(8) Å. The carborane *m*CB-L linker shows a V-shape (OOC–CBcentroid–COO ≈ 115°) and two noncoplanar phenyl rings (70°). In this structure, each Cu_2-paddlewheel cluster is connected to four *m*CB-L ligands forming planar 2D layers with a 4^4-grid topology (Figure 2b). Interestingly, the later layers where highly corrugated in the related structure where DABCO was not incorporated.[58] In ***m*CB-MOF-1**, the observed 2D layers are flat and linked by the pillaring DABCO ligand with a N-N distance of 2.573(8) Å, giving rise to the 5-connected 3D structure shown in Figure 2c. Quite remarkably, the DABCO ligands coordinate to only one of the two apical sites of each Cu_2-paddlewheel cluster and alternate above and below the Cu_2-paddlewheel/*m*CB-L layers (Figures 2b-c). This provides large rectangular channels (18.6 x 4.2 Å), in which the apical positions of the Cu_2-paddlewheel units are occupied by water molecules. These large rectangular channels are minimized by a 2-fold interpenetration of another 5-connected network, providing square 1D channels (Figure 2d) of about 7.0 x 7.0 Å when coordinated water is excluded. The interpenetrated networks are interacting by π-stacking interactions between the centroids of the aromatic rings (3.7174(2) Å) and with an angle of 9.70(14) º between their planes (Figure S4). Such interpenetration is unusual when a small pillar ligand such as DABCO is employed.[59-60]

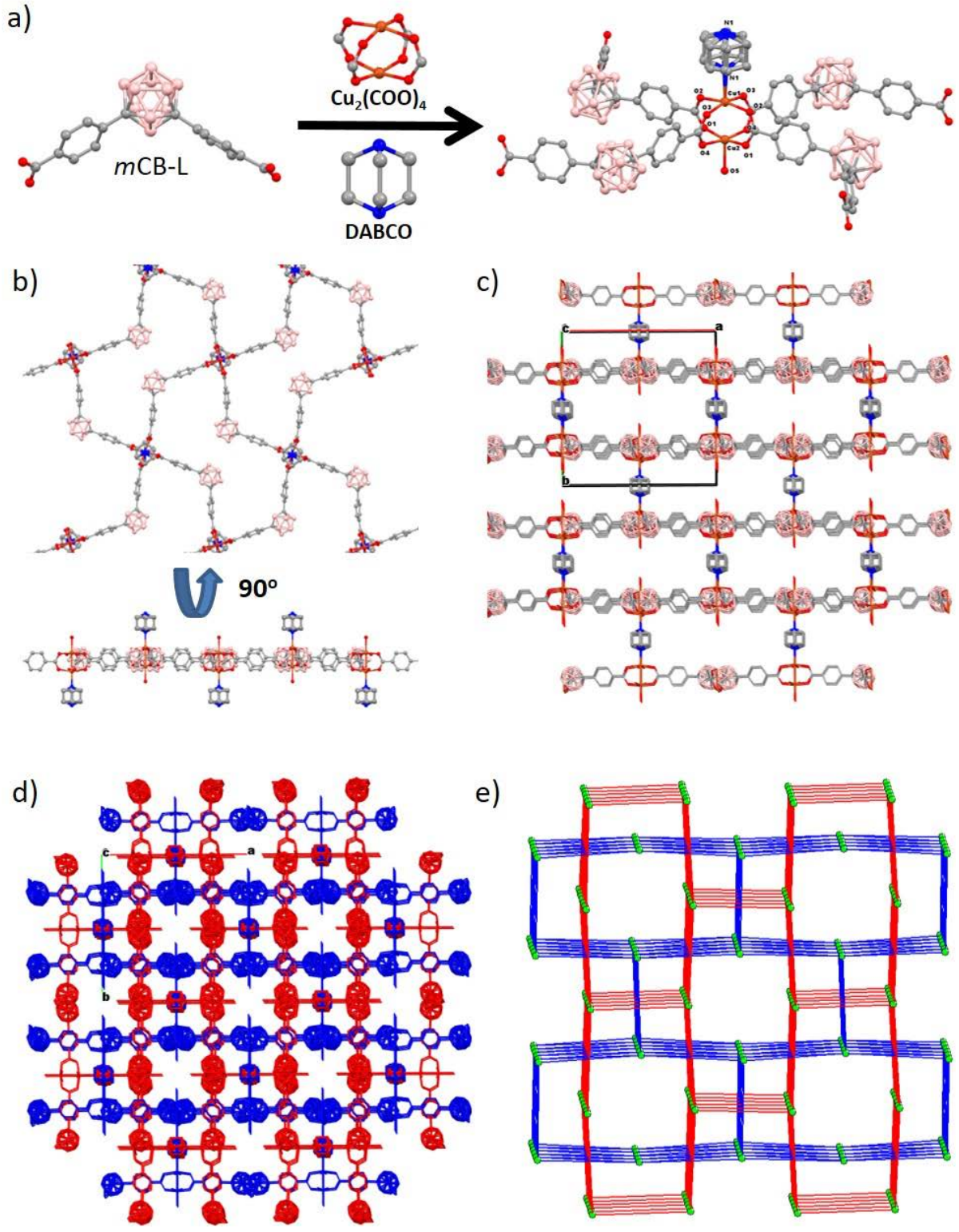

Figure 2. Crystal structure of ***m*CB-MOF-1**. a) View of the Cu_2-paddlewheel units with *m*CB-L coordination. b) Two perpendicular views of the extended structures showing the 2D 4^4 networks. c) 3D framework having a 5-connected $(4^4)(6^6)$ topology with rectangular 1D channels. d) 2-fold

interpenetrated structure with square 1D channels. e) Underlying 2-fold interpenetrated 5-connected nets in the structure of ***m*CB-MOF-1**; green spheres represent the Cu_2-paddlewheel cluster nodes. Interpenetrated networks are colored differently for clarity. H atoms are omitted for clarity. Color code: B pink; C grey; O red; N blue, Cu orange.

The structure of ***m*CB-MOF-1** is a rare example of 5-connected $(4^4)(6^6)$ topology[61-62] (sqp) and represents the first example of such a topology in a Cu_2-paddlewheel MOF. Indeed, the $Cu_2(O_2CR)_4A_2$ (A = apical ligands) paddlewheel units serve as lineal, square or octahedral building units, if all dimer cluster coordination sites are occupied by polytopic ligands (i.e., saturated).[63] In the case of ***m*CB-MOF-1**, the apical positions for each Cu_2-paddlewheel are occupied by a nitrogen atom of one DABCO and oxygen from water molecules. This rare structural topology[64-66] allows the activation of ***m*CB-MOF-1** by removal of the Cu-coordinated water, leading to an open porous structure.

The bulk phase and analytical purity of the as made ***m*CB-MOF-1** were confirmed by powder X-ray diffraction (PXRD, Figure 3), elemental analysis, thermogravimetric analysis (TGA) and infrared spectroscopy. TGA of the as-synthesized ***m*CB-MOF-1** after washing with DMF followed by soaking in acetone revealed a plateau in the range 100-300 ºC (Figure S5). Variable temperature Synchrotron Wide Angle X-ray Scattering (WAXS) measurements showed that ***m*CB-MOF-1** retains its original structure up to 300 ºC under dynamic vacuum (Figure S6). Upon activation at 130 ºC for 12 h under vacuum, the TGA profile of our material confirms that all guest molecules are successfully removed from the pores and provided the activated ***m*CB-MOF-1'**. PXRD studies revealed that the structure of the activated ***m*CB-MOF-1'** is intact upon removal of the guest molecules from its cavities (Figure S3). Type I N_2 isotherms collected at 77K and 1 bar confirmed the microporous nature of ***m*CB-MOF-1'** and the BET surface area and pore volume were found to be 756 m^2g^{-1} and 0.31 cm^3/g, respectively (Figure 3a and Table S2). ***m*CB-MOF-1'** is also porous to CO_2 (1.34 mmol g^{-1}) at 313 K and 2 bar (Figure S7).

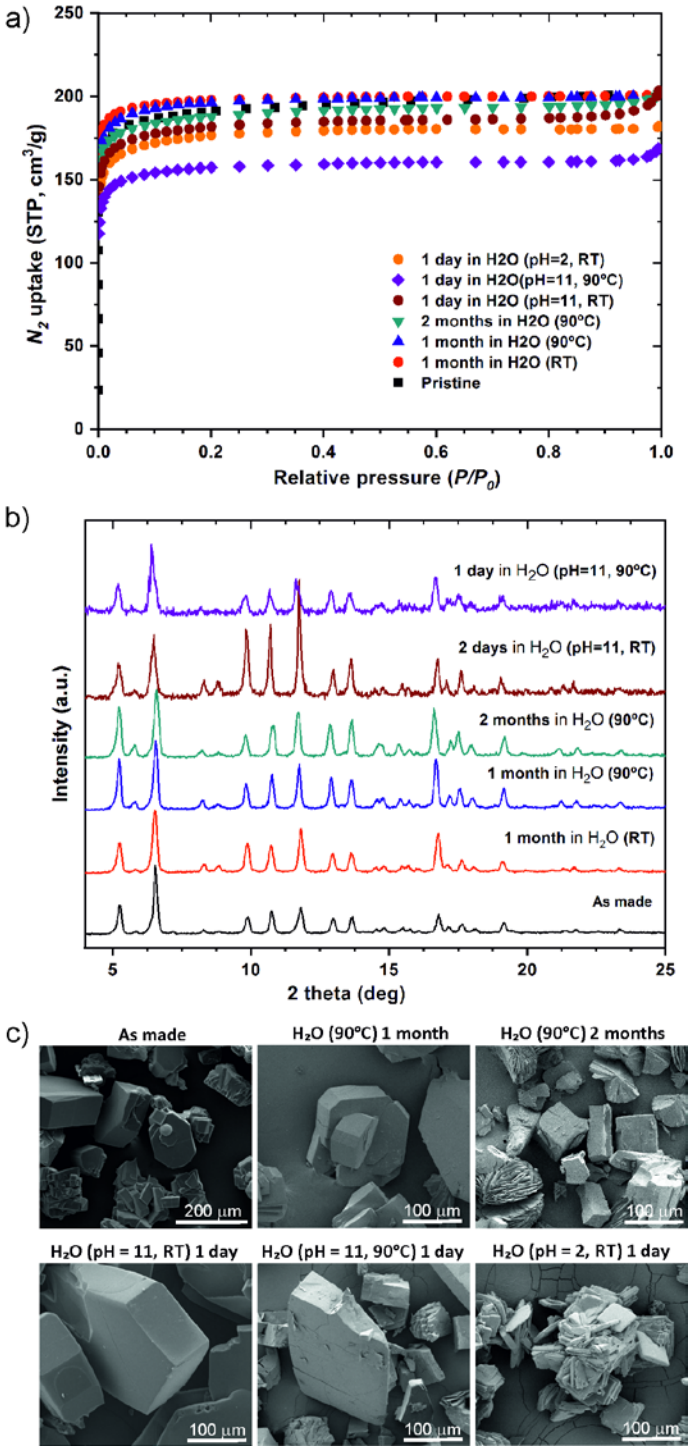

Figure 3. Comparison of the a) N_2 adsorption isotherms at 77 K and b) PXRD patterns for activated ***m*CB-MOF-1'** and after being in water at various conditions. c) Scanning Electron Microscopy (SEM) images showing crystals morphology of as made ***m*CB-MOF-1** and that of ***m*CB-MOF-1'** after being in water at the indicated conditions.

***m*CB-MOF-1** represents a rigid two-fold interpenetrated porous structure and PXRD studies show that no structural changes can occur upon activation (Figure S3) or upon its immersion in a variety of organic solvents such as alcohols, benzene, toluene and acetonitrile (Figure S8). The rigidity of ***m*CB-MOF-1'** can be attributed to the observed π-stacking interactions of the interpenetrated networks of ***m*CB-MOF-1**. The interpenetration[67] and formation of π-stacking motifs[26, 68] are known to provide overall stabilization. We reasoned that such rigid structure could also be stable in water as the highly hydrophobic carborane moieties are decorating the MOF channels, thus providing protection to the Cu_2-paddlewheel units against hydrolysis or ligand displacement (Figure 4).[42, 44]

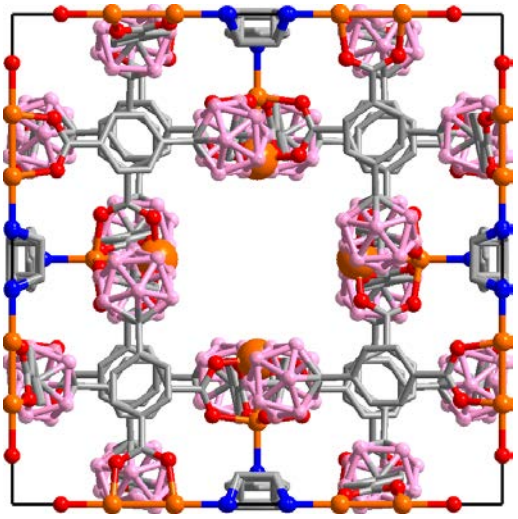

Figure 4. A 3D view of the crystal structure of ***m*CB-MOF-1** along the *c* axis showing the environment of four Cu atoms (enlarged orange spheres) in the channels. Color codes: Boron, pink; carbon, grey; nitrogen, blue; oxygen, red. H atoms are omitted for clarity.

Hydrolytic stability and hydrophobicity. It is noteworthy that ***m*CB-MOF-1'** is stable when incubated in liquid water for at least one month at room temperature. More strikingly, it is fully stable in hot water (90 ºC) for up to one month as proved by a combination of PXRD, BET, SEM and ICP measurements (Figure 3a-b and Table S2). Indeed, PXRD traces of ***m*CB-MOF-1** before and after incubation for two months at 90 ºC in water in a closed vial perfectly match the simulated pattern derived from the single crystal structure of ***m*CB-MOF-1** (Figure 3b). However, there is a

clear consensus that providing only the PXRD as a proof for water stability is not acceptable, and other experimental evidences, such as gas sorption isotherms and SEM are mandatory to confirm its water stability.[69] Thus, the stability of ***m*CB-MOF-1** was also confirmed by N_2 adsorption measurements of the solids after water treatment. Porosity is retained as proved by the BET surface area measurements of the treated samples (Figure 3a and Table S2). Samples after water treatment for up to two months at 90 ºC show negligible changes in their surface area and pore volumes compared with the as made material (see Table S2 for details). SEM images of both ***m*CB-MOF-1** and ***m*CB-MOF-1'** after their immersion in water at 90 ºC for one month show no significant morphology change of the polyhedral block crystals nor evidence of surface cracking (Figure 3c and Figure S9). No significant weight loss was observed for the samples treated under the above described conditions and consequently, copper leaching is deemed negligible in all the cases (see Table S2 for details).

Moreover, ***m*CB-MOF-1'** is also stable when incubated in liquid water over a wide pH range (from 2 to 11; pH adjusted with HCl or NaOH) for at least 48 h at room temperature (Figure 3 and S10). PXRD patterns show that ***m*CB-MOF-1'** is more stable in basic than in acid conditions (Figure S10). After immersion in water at pH 2, the surface area and pore volume of ***m*CB-MOF-1'** decreases from 756 to 698 m^2g^{-1} and 0.31 to 0.28 cm^3g^{-1} in one day (Table S2). While in basic conditions (water, pH 11), the surface area and pore volume of ***m*CB-MOF-1'** decreases from 756 to 722 m^2g^{-1} and 0.31 to 0.30 cm^3g^{-1} in one day. Longer exposure to the above conditions shows a decrease in its surface area and pore volume (see Table S2 for details). SEM images of the samples immersed in acidic or basic conditions (Figure 3C and S11) show a clear change in morphology from polyhedral crystals to small plates in the samples being in acidic aqueous solution but no morphology changes are observed in the samples being in basic conditions. The higher stability of ***m*CB-MOF-1'** in basic aqueous solutions prompted us to study the stability under harsher conditions. Remarkably, ***m*CB-MOF-1'** is also stable in basic conditions (pH 11) at 90 ºC for at least 24h (Figure 3 and S10). When heated under basic conditions for 24h, slight structural changes are already visible (Figure 3b). The PXRD pattern for ***m*CB-MOF-1'** after being at 90 ºC in water (pH 11) for one day shows a slight decrease in intensity of peaks at 2θ = 8.3, 8.8, 14.5, 14.8 and 15.4 and we observed no additional peaks at higher angles (Figure S12). Consistently, SEM images clearly show the presence of cracks on the surface of the polyhedral crystals and the appearance of some spherulites (Figure 3c and S11).[70-71] The presence of spherulites in the SEM images of the

treated ***m*CB-MOF-1'** does not reflect a significant change in the PXRD data with respect to the PXRD pattern of the as made material. The treated material under basic conditions still shows high porosity (629 m^2g^{-1} at 77 K, Figure 3 and Table S2) with a pore volume of 0.26 cm^3g^{-1}. Quite surprisingly, copper leaching after such hard conditions was practically negligible (476 ppb) as determined by ICP.

As reasoned above, we attribute this remarkably high hydrolytic stability to a combination of interpenetration and the hydrophobic nature of the *meta*-carborane residues in the structure ***m*CB-MOF-1**, which hinder the degradation of the Cu_2-paddlewheel units (Figure 4). Shimizu and coworkers have recently provided a way to parametrize and grade the hydrolytic stability of MOFs, based on structural and sorption properties.[69] These authors proposed six levels of hardness to water exposure (1 to 6: ambient conditions to boiling water) and four categories (A to D: retention of crystallinity and porosity to loss of porosity and crystallinity) as a way to benchmark both with respect to how the MOF was treated and the post-treatment analysis. Using this stability level, HKUST-1 is classified with a 4B stability (retained some porosity but losses some order when immersed in water), DMOF is classified as 3D (loss of porosity and crystallinity when exposed to intermediate humid conditions), whereas MIL-53 and ZIF-8 are classified as 6B and 6C, respectively (retained some porosity or some order when immersed in boiling water). Following this classification, our Cu_2-paddlewheel MOF ***m*CB-MOF-1** correspond to 6A stability which is, to our knowledge, the highest hydrolytic stability of a Cu-based MOF and surpasses that of the well-known families of ZIF- or Zr-MOFs (Table S3).[69, 72]

Having determined that ***m*CB-MOF-1** is robust and permanently porous, we then evaluated the influence of the carborane units on its hydrophobic properties. The water adsorption isotherm for ***m*CB-MOF-1'** collected at 313 K (Figure 5) exhibits a type-II sorption isotherm, typical of a material with low affinity for water; this is in agreement with the hydrophobic nature of the *m*-carborane residues present in ***m*CB-MOF-1**.[73] We then performed water contact-angle measurements of dry ***m*CB-MOF-1'** in crystalline powder packed on a glass surface and in the form of a disk pellet (diameter = 13 mm), which was fabricated by pressing a dry crystalline powder under a pressure of 10 tons for 5 min.[74] The contact angle (Θ_c) in each case was 144° and 101°, respectively — values which are characteristic of a hydrophobic solid. ***m*CB-MOF-1'** shows a similar hydrophobicity to that of the other highly hydrophobic MOFs (*e.g.* ZIF-8, Θ_c = 142º).[75] We also quantified the contact-angle hysteresis (CAH) that was found to be 32° (Supporting

Information, Table S3). This CAH was attributed to the surface roughness of the disk pellet that can be the responsible for the contact line pinning.[76] Additionally, if a glass substrate bearing ***m*CB-MOF-1'** powder was inclined after placing a droplet of water on its surface, a ***m*CB-MOF-1'**-covered water droplet (known as *liquid marble*) was formed (Figure S13); this is known to be a common occurrence with hydrophobic powders.[76]

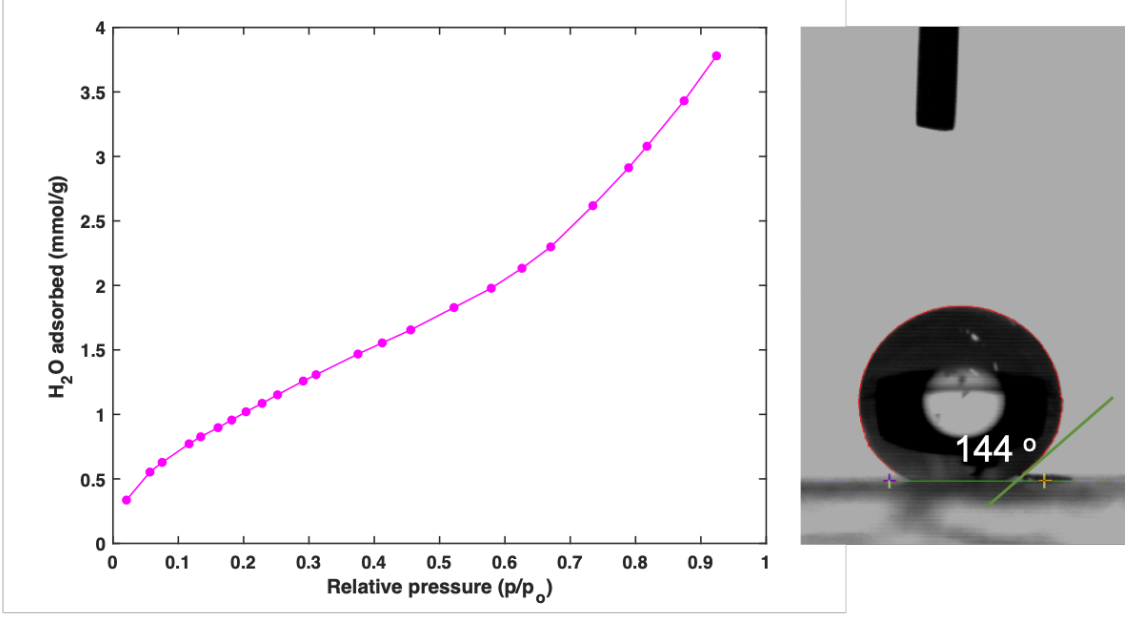

Figure 5. Left: Type II water vapor adsorption collected on ***m*CB-MOF-1'** at 313 K, and right: water contact angle photo of a crystalline powder packed on glass surface.

Butanol separation. The permanent porosity, type II water isotherms and excellent hydrolytic stability of ***m*CB-MOF-1** prompted us to check the performance of this MOF towards butanol separation from realistic multicomponent aqueous mixtures. With this aim, we proceeded to evaluate the accessibility of its pore structure to the ABE mixture by means of **i.** equilibrated single component vapor isotherms, **ii.** dynamic variable temperature pulse gas chromatography and **iii.** integrated gas stripping-dynamic vapor phase breakthrough curve measurements collected at 333 K. In order to put the results into a broader context, we compared the performance of ***m*CB-MOF-1** with that of the well-known ZIF-8, which is a highly porous (BET surface area: 1630 m^2g^{-1}), stable and hydrophobic material.

With this aim, single-component vapor phase adsorption isotherms of butanol and ethanol were measured for ***m*CB-MOF-1** and ZIF-8 at 313 K and acetone at 303 K (Figures 6). The results

show significant differences between these two materials in terms of their uptake capacities and uptake behavior of alcohols. Firstly, in accordance with their respective porosity features, ZIF-8 exhibits higher saturation uptake for all alcohols which is attributed to its higher surface area and pore volume. Secondly, ***m*CB-MOF-1** and ZIF-8 behave differently at the critical low-pressure region: there is a steep uptake when ***m*CB-MOF-1** is used, and there is a negligible uptake when ZIF-8 is used. The type I vapor isotherms for butanol, ethanol and acetone indicate that the pores in ***m*CB-MOF-1** are readily accessible for these molecules to diffuse in and therefore, ***m*CB-MOF-1** forms strong interactions with these molecules (Figure 6a). Whereas, as shown in Figure 6b, ZIF-8 exhibits the characteristic sigmoidal S-shaped isotherms for the alcohol vapors, indicating weak interactions between the ZIF-8 and alcohols at the low-pressure region; biobutanol and other alcohol products are typically dilute solutions in water. In addition, the absence of hysteresis in the isotherms collected on ***m*CB-MOF-1** facilitates the easier desorption of the adsorbed alcohols.

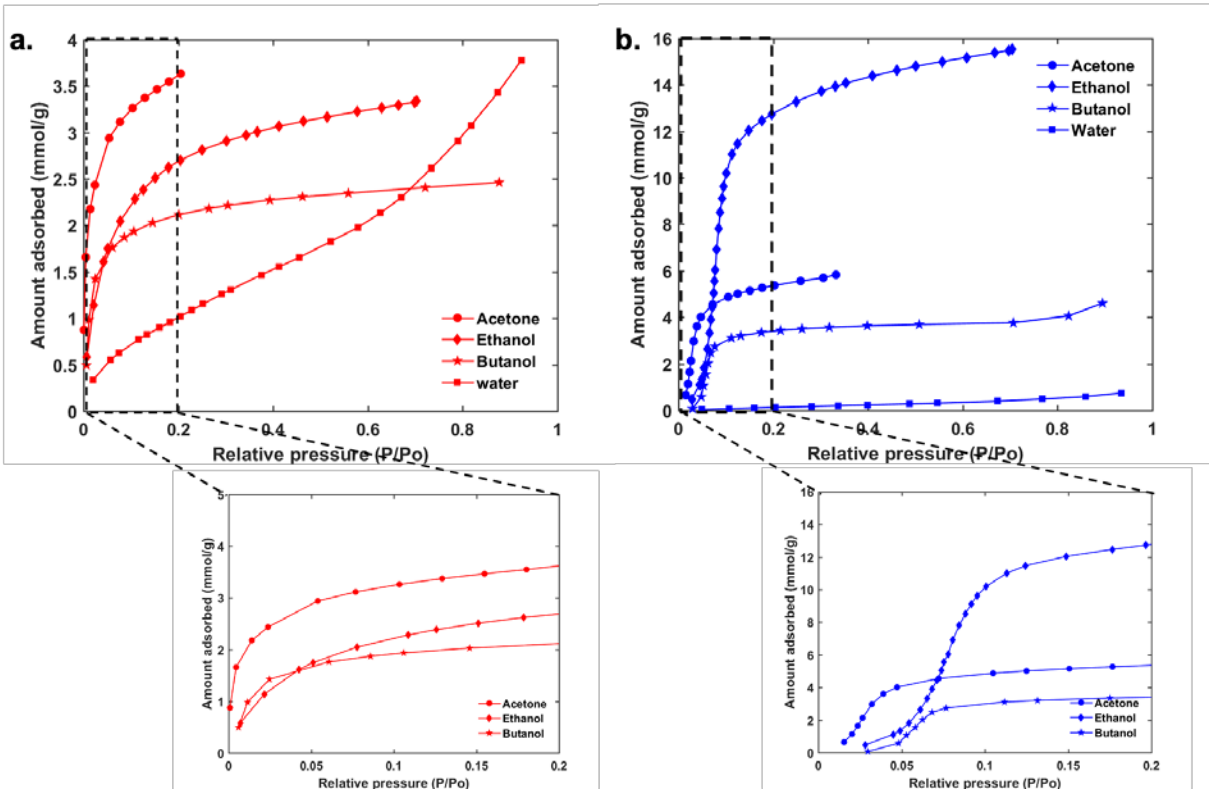

Figure 6. Acetone (303 K), butanol and ethanol (313K) vapor isotherms collected on ***m*CB-MOF-1'** (a) and ZIF-8 (b).

The selectivity of butanol over ethanol was evaluated using the Ideal Adsorbed Solution Theory (IAST).[77] Predictions show a much higher uptake of butanol over ethanol in both ***m*CB-**

MOF-1' and ZIF-8. Remarkably, a higher butanol uptake is observed in ***m*CB-MOF-1'** than in ZIF-8 in the low-pressure region, and contrary to the latter, ***m*CB-MOF-1'** shows a negligible ethanol uptake over all pressure range (Figure S14a-b). The selectivity results of ***m*CB-MOF-1'** for butanol over ethanol shows higher than 12.0 in the < 25 kPa and decrease slowly to 7.0 at 100 kPa, being overall larger than that for ZIF-8 (Figure S14c). Consequently, the overall behavior is in agreement with a higher butanol/ethanol selectivity for ***m*CB-MOF-1'**.

To further characterize the alcohol-MOF interactions, gas-phase pulse chromatographic were performed (Figures S15-16). Both ***m*CB-MOF-1** and ZIF-8 were packed in separate columns and the experiments were performed at 443 K and 503 K. A broad peak for butanol can be seen in Figure S16, which suggests a relatively strong adsorbate (butanol)-adsorbent (***m*CB-MOF-1**) interactions. This can be explained by the slow intracrystalline diffusion of the butanol molecules after they diffuse in the pores. To the contrary, acetone peaks are symmetrical for both ZIF-8 and ***m*CB-MOF-1** suggesting that the acetone molecules are not obstructed by intracrystalline diffusion. NMR experiments were also performed to evaluate the multicomponent vapour uptake capacity of both MOFs. Under atmospheric pressure and at 333 K, we observed that both ZIF-8 and ***m*CB-MOF-1** uptake comparable amounts of butanol regardless of the difference in their BET surface areas. (Table S7).

Having established the single component interactions of ABE components with the porous framework, we then proceeded to study the butanol separation under industrially relevant conditions in order to evaluate the effect of competitive adsorption of the different components. With this aim, we studied the separation of butanol through an integrated gas stripping-adsorption process with a model aqueous solution of ABE mixture (composition: acetone 7.04g/l, 0.715wt%; butanol 13.75g/l, 1.39wt%; ethanol 2.56g/l, 0.26wt%; water 960.69g/l, 97.63wt%). 1000 mL of the ABE mixture was thermostatized at 313 K and bubbled with He flow (40 mL min^{-1}). The resulting flow of He, which carried the ABE vapor, was fed as the inlet stream to a thermostatized chromatographic column (4 mm inner diameter/10 cm long) packed with ***m*CB-MOF-1** or ZIF-8 and maintained at 333 K. It is worth mentioning that the standard ABE fermentation temperature of solventogenic clostridium species in the bioreactor ranges from 308 to 313 K. It is well demonstrated that any operating temperature above 313 K will hamper the production and yield, as it negatively affects the clostridium species. Thus, in our proposed integrated process illustrated in Figure 1, we envision that the ABE vapor generated in the bioreactor in concordance with the

standard operating conditions of 313 K and 1 atmosphere pressure is stripped by a carrier gas from the headspace of the reactor, and the resultant ABE vapor is externally heated to 333 K before being fed to the fixed adsorbent bed. We chose to set up the temperature of our sorption column at 333 K owing to the observation of comparatively very low adsorption and the concomitant rapid elution of the raffinate – acetone and ethanol from sorption column loaded with ***m*CB-MOF-1** (Figure S17). This finding from a lab scale setup, when extrapolated to an industrial scale process, is considered to be highly meritorious in terms of the overall downstream separation process efficiency and the associated process engineering and economics – capital and operating costs requirements. Thus, the breakthrough curves collected on ***m*CB-MOF-1** and ZIF-8 are presented in Figure 7.

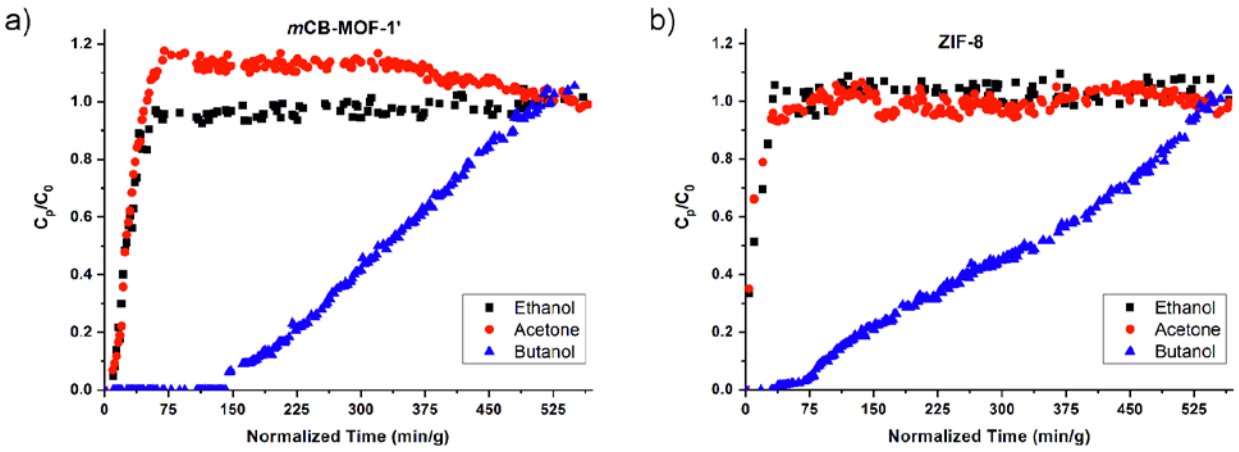

Figure 7: Breakthrough curves collected at 333K on ***m*CB-MOF-1' and ZIF-8**. Color code: red: acetone, black: ethanol and blue: butanol.

The breakthrough curves indicate that at 333 K, acetone, ethanol and butanol are initially co-adsorbed, however, after acetone and ethanol become saturated, butanol replaces these weakly adsorbed components. As can be seen in Figure 7, ***m*CB-MOF-1'** performs better than ZIF-8 as exemplified by the respective breakthrough times of 146 and 80 min/g respectively, which correlates to their adsorption capacity (butanol) at low pressure and strength of adsorbate-adsorbent interactions. It can be therefore, concluded that the butanol interactions with ***m*CB-**

MOF-1 pore framework gives rise to a material which can recover butanol from the ABE mixture at 333 K more efficiently compared to ZIF-8.

To gain insights on the adsorption of butanol, ethanol or acetone in ***m*CB-MOF-1'**, we conducted Monte Carlo simulations. The results indicate that all three molecules preferentially distribute within the pockets created by the 2-fold interpenetrated structure and away from the 1D channels of ***m*CB-MOF-1'** (Figure S18). A larger amount of intermolecular contacts between butanol and the phenyl rings in the pockets than acetone or ethanol can explain the relatively stronger interaction between ***m*CB-MOF-1'** and the larger alcohol (Figure S18). The binding energies of those interactions have been calculated by DFT and compared with that for ZIF-8 (Table S8). The results show that the binding energy of butanol is greater than those for acetone or ethanol in both MOFs. However, the binding energy of butanol with ***m*CB-MOF-1'** (-78.00 kJ/mol) is larger than the corresponding energy for ZIF-8 (-48.43 kJ/mol). These results are in agreement with the shape of the single isotherms for both MOFs (Figure 6) and support the observed higher selectivity of butanol over ethanol for ***m*CB-MOF-1** than for ZIF-8 (Figure S14c). The higher number of H atoms in the larger alcohol can improve the interactions between the small pores (0.7 nm) of ***m*CB-MOF-1'**, whereas those are disfavored in the larger pores (1.1 nm) of ZIF-8. The small pores of our carborane based MOF are fully decorated with low polar B-H groups and nonpolar phenyl rings and that might certainly explain the preferential adsorption of butanol molecules.

Conclusions

In summary, a new Cu(II) based porous MOF (***m*CB-MOF-1**) has been synthesized and characterized. The activated ***m*CB-MOF-1'** is porous and stable in both basic and acidic aqueous solutions as confirmed by PXRD, BET surface areas, SEM images and ICP. ***m*CB-MOF-1'** is stable in water at 90 ºC for over two months and also stable when incubated in liquid water over a wide pH range (from 2 to 11) for at least 48 h at room temperature and it is also stable in basic conditions (pH 11) at 90 ºC for at least 24h. Such hydrolytic stability is attributed to a combination of interpenetration and the highly hydrophobic nature of the *meta*-carborane residues in the structure ***m*CB-MOF-1**, which hinder the degradation of the Cu_2-paddlewheel units. Contact angle and water vapor isotherms indicated that ***m*CB-MOF-1** exhibits hydrophobicity on both the

external crystal surfaces (Θ_c = 144 º) and the internal pores (type-II water sorption isotherm). Based on the properties of ***m*CB-MOF-1**, we tested this material towards butanol recovery from the ABE mixture. Single-component adsorption isotherms of acetone, butanol and ethanol for ***m*CB-MOF-1** afforded type I isotherms in the low-pressure region, indicative of a strong affinity for the components of the ABE mixture. The selectivity of ***m*CB-MOF-1'** for butanol over ethanol, calculated by the Ideal Adsorbed Solution Theory, shows higher than 12.0 in the < 25 kPa and only slowly decrease to 7.0 at 100 kPa, being overall larger than that for ZIF-8. Monte Carlo and DFT calculations show that our MOF has higher affinity for butanol than ZIF-8, and show that the adsorbates preferentially distribute within the pockets created by the 2-fold interpenetrated structure of ***m*CB-MOF-1'**. We therefore investigated the separation performance of ***m*CB-MOF-1** for ABE aqueous solution (acetone 7.04g/l, 0.715wt%; butanol 13.75g/l, 1.39wt%; ethanol 2.56g/l, 0.26wt%; water 960.69g/l, 97.63wt%.) separation by an integrated process of gas stripping-vapor phase adsorption process with dynamic breakthrough experiments and compared the separation performance with ZIF-8 under the same conditions. Due to the stronger butanol-***m*CB-MOF-1'** interactions, breakthrough curves showcase that ***m*CB-MOF-1'** recovers butanol more efficiently compared to ZIF-8 at 333 K. Our work demonstrates a step forward towards the discovery of novel water stable MOFs for biobutanol recovery from a mostly water-containing ABE mixture. To date, only ZIFs have been tested towards this application and based on our findings, carborane-based MOFs can compete with ZIFs and can even outperform them in the separation of biobutanol. Future work includes the scale up of ***m*CB-MOF-1** synthesis, shape engineer its powder form into a more industrially favored form, and test its performance using different bed configurations as dictated by process modelling.

EXPERIMENTAL SECTION

Materials. 1,7-di(4-carboxyphenyl)-1,7-dicarba-*closo*-dodecaborane ligand (*m*CB-H_2L) was synthesized according to the literature procedure.[78] Synthesis of ***m*CB-MOF-1** was done in air. All chemicals were commercially available and used as received.

Synthesis of $[Cu_2(mCB\text{-}L)_2(DABCO)_{0.5}(H_2O)]\cdot 2DMF\cdot 2H_2O$ **(*m*CB-MOF-1)**. *m*CB-H_2L (90 mg, 0.234 mmol), DABCO (6.5 mg, 0.059 mmol), DMF (5 mL) and H_2O (1 mL) were added to an 8-dram vial and the mixture was sonicated until dissolution of the solids. Next, an ethanol

solution (5 mL) of $Cu(NO_3)_2$•$6H_2O$ (68 mg, 0.234 mmol) was added to the mixture. The vial was closed and heated at 80 °C in an oven for 48 h, followed by slow-cooling to room temperature for 5 h. Greenish crystals of ***m*CB-MOF-1** were collected and washed with DMF (100 mg, yield 50 %). IR (ATR; selected bands; cm-1): 2601 (BH); 1716 (C=O from carboxylate). Elemental analysis (%) calculated for $C_{41}H_{32}B_{20}Cu_2NO_9$: C 42.67, H 4.54, N 3.64; Found: C 42.68, H 4.97, N 3.59.

As synthesized ***m*CB-MOF-1** crystals were immersed in acetone (20 mL) and replaced once a day for three days, filtered and dried in air. The later was then activated by heating at 130 ºC under dynamic ultrahigh vacuum for 12h.

Hydrothermal stability Tests. Solvent-exchanged and fully activated ***m*CB-MOF-1'** was used for all hydrothermal stability tests. All experiments were replicated and the conditions were chosen to test stability in liquid water at room temperature and at 90 ºC in closed vials inside an oven (Table S2). Such heating conditions were chosen as a more reproducible method than that for the unspecific "boiling water" methods reported in the literature. Samples treated under the different conditions, were filtered, and dried in air. Stability of the treated samples was evaluated by X-ray diffraction, and BET of activated samples. Selected water treated samples were further analyzed for Cu content by ICP or SEM images.

Breakthrough experiments. MOFs (500 mg) were packed into a stainless steel column (10 cm long; 4 mm internal diameter) and activated by heating overnight at 403K under a Helium flow (40ml/min) before measurements. Breakthrough measurements were done as follows: a continuous He flow (40 ml/min) was bubbled through the ABE mixture (acetone 7.04 g/l, 0.715 wt%; *n*-butanol 13.75 g/l, 1.39 wt%; ethanol 2.56 g/l, 0.26 wt%; water 960.69 g/l, 97.63 wt%), thermostatized at 313K, the forming stream subsequently was flow through the MOF (***m*CB-MOF-**1 or ZIF-8) packed in the column at 333K.

NMR experiments. We performed loading experiments (comparable with the breakthrough experiments above) using a 10 cm long, 4 mm internal diameter home-made glass column and nitrogen as gas carrier (flow, 40 ml/min). The loading experiments were performed on ***m*CB-MOF-1'** (500 mg) and ZIF-8 (450 mg) at 333 K and atmospheric pressure. After 570 mins, the corresponding MOFs' adsorbates were extracted with $CDCl_3$ and the concentration of each molecule was determined by NMR, using benzene as an internal standard. The results are summarized in Table S7.

Characterization and methods.

Attenuated total reflection Fourier transformed infrared (ATR-FTIR) spectra were recorded using a PerkinElmer Spectrum One spectrometer equipped with a Universal ATR sampling accessory. Spectra were collected with 2 cm^{-1} spectral resolution in the 4000-650 cm^{-1} range. Elemental analyses were obtained by using a Thermo (Carlo Erba) Flash 2000 Elemental Analyser, configured for wt.%CHN. Thermogravimetric Analysis (TGA) was performed in N_2, on an nSTA 449 F1 Jupiter-Simultaneous TGA-DSC or SDT Q600 V8.3 Build 101 instruments (heating rate: 5 ºC/min; temperature range: 25 ºC to 600 ºC). Gas sorption-desorption (CO_2/273 K and N_2/77 K) measurements were performed using IGA001 and ASAP2020 surface area analyzer. The sample was first degassed at 130 °C for 12 h. Crystals for X-ray Diffraction (XRD) were prepared under inert conditions immersed in perfluoropolyether or paratone as protecting oil for manipulation. Suitable crystals were mounted on MiTeGen Micromounts^{TM}, and used for data collection at BL13 (XALOC)[79] at the ALBA synchrotron with an undulator source and channel-cut Si(111) monochromator and Kirkpatrick-Baez focusing mirrors with a selected wavelength of 0.72932 Å. An MD2M-Maatel diffractometer fitted with a Dectris Pilatus 6M detector was employed. The sample was kept at 100 K with an Oxford Cryosystems 700 series Cryostream. The structure was solved with the ShelXT 2014/5 (Sheldrick, 2014) structure solution program using the direct phasing methods solution method and by using **Olex2** as the graphical interface.[80] The model was refined with version 2016/6 of **ShelXL** using Least Squares minimisation.[81] Highly disordered solvent, identified as 6 ethanol per formula unit, was treated using a solvent mask (Squeeze). A summary of crystal data is reported in Table S1 in the SI. Powder X-ray Diffraction (PXRD) was recorded at room temperature on a Siemens D-5000 diffractometer with Cu Kα radiation (λ = 1.54056 Å, 45kV, 35mA, increment=0.02º). Morphological features were examined first by optical microscopy and subsequently by scanning electron microscopy (SEM) with a QUANTA FEI 200 FEGESEM microscope. Water contact-angles were measured using a Krüss DSA 100 device at room temperature using water as the probe fluid (9 μL). Inductively Coupled Plasma – Mass Spectrometry (ICP-MS) measurements were carried out in an Agilent ICP-MS 7700x apparatus. Water, ethanol and butanol adsorption isotherms were measured at 313 K while acetone isotherms were collected at 303 K using the Microtrac BELSORP aqua^3 instrument. ^{1}H NMR spectra were recorded on a Bruker Advance DPX-360 MHz spectrometer in deuterated chloroform, and referenced to the residual solvent peak.

WAXS patterns were recorded on the NCD-SWEET beamline at ALBA synchrotron light source (Spain). An X-ray beam of 8 keV (λ = 1.54 Å) was set using a Si (111) channel cut monochramator. The scattered radiation was recorded using a Rayonix LX-255HS area detector. The sample to detector distance and the reciprocal space calibration were obtained using Cr_2O_3 as a standard calibrant. The MOF was introduced in a borosilicate capillary and heated until 300 ºC using a Linkam TMS-350 capillary stage (10 ºC/min from 25 ºC; resting 30 minutes after every 50 ºC increase) under dynamic vacuum. Data reduction from 2D images to 1D profiles via azimuthal integration was done using PyFAI.[82]

The isothermal parameters were well fitted by the Lagmuir-Freundlich (LF) method from the pure adsorption isotherms at 313K.[83-84] Fitting parameters of LF equation as well as the correlation coefficients (R^2) are listed in Tables S5-S6. Predicted isotherms and Selectivity for mixtures of butanol and ethanol (0.85:0.15) at 313K was analyzed using IAST (Figure S14a-c).

Adsorbate location. In order to localize the positions of the butanol, ethanol or acetone molecules within the ***m*CB-MOF-1'** pores, the Adsorption Locator module of the Materials Studio 6.0 software[85] was employed to perform Monte Carlo simulations. The used forcefield was COMPASS,[86] the charge was forcefield assigned and the summation methods were group- and atom-based. The simulations yielded the most stable conformation of the butanol, ethanol or acetone molecules within the pores of ***m*CB-MOF-1'**.

Binding energy calculation. Periodic DFT calculations were carried out using the CP2K code.[87] All calculations employed a mixed Gaussian and planewave basis sets. Core electrons were represented with norm-conserving Goedecker-Teter-Hutter pseudopotentials,[88-90] and the valence electron wavefunction was expanded in a double-zeta basis set with polarization functions[91] along with an auxiliary plane wave basis set with an energy cutoff of 400 eV. The generalized gradient approximation exchange-correlation functional of Perdew, Burke, and Enzerhof (PBE)[92] was used. Test calculations showed that the total energy change of the reactive system was negligible (<0.01 eV) when the maximum force convergence criteria of 0.001 hartree/bohr was used. Each reaction state configuration was optimized with the Broyden-Fletcher-Goldfarb-Shanno (BGFS) algorithm with SCF convergence criteria of 1.0×10^{-8} au. To compensate the long-range van der Waals dispersion interaction between the adsorbate and the MOF, the DFT-D3 scheme[93] with an empirical damped potential term was added into the energies obtained from exchange-correlation

functional in all calculations. The value of binding energies (BE) were calculated as the energy difference before and after adsorption in the adsorption process, as defined by

$$BE = E_{MOF+vapor} - E_{MOF} - E_{vapor}$$

where $E_{MOF+vapor}$ is the total energy of the MOF/ABE adsorption system in equilibrium state, while E_{MOF} and E_{vapor} are the energy of the adsorbate-free MOF structures and the vapor adsorbate, respectively. A negative value of BE suggests an exothermic adsorption of the vapor molecule over MOF.

ASSOCIATED CONTENT

Supporting Information

The Supporting Information is available free of charge at https://pubs.acs.org/doi/xxxx.

Single-crystal X-ray data (CCDC no. 1966753) (CIF), photographs, IR, Crystallographic data, PXRD, TGA, WAXS, sorption isotherms, SEM images, IAST details, pulse gas chromatograms, NMR, breakthrough curves at various temperatures, Monte Carlo simulations and DFT calculations (PDF)

AUTHOR INFORMATION

Corresponding Authors

José Giner Planas – *Institut de Ciència de Materials de Barcelona (ICMAB-CSIC) Bellaterra, Spain. E-mail: jginerplanas@icmab.es*

Kyriakos C. Stylianou – *Institute of Chemical Sciences and Engineering, École Polytechnique Fedérale de Lausanne (EPFL Valais), Rue de l'Industrie 17, 1951 Sion, Switzerland, and Department of Chemistry, Oregon State University, 153 Gilbert Hall, OR 97331, Corvallis, Oregon, USA. E-mail: kyriakos.stylianou@oregonstate.edu*

Authors

Lei Gan – *Institut de Ciència de Materials de Barcelona (ICMAB-CSIC) Bellaterra, Spain.*

Arunraj Chidambaram – *Institute of Chemical Sciences and Engineering, École Polytechnique Fedérale de Lausanne (EPFL Valais), Rue de l'Industrie 17, 1951 Sion, Switzerland.*

Pol G. Fonquernie – *Institut de Ciència de Materials de Barcelona (ICMAB-CSIC) Bellaterra, Spain.*

Mark E. Light – *Department of Chemistry, University of Southampton, Highfield, Southampton SO17 1BJ, UK.*

Duane Choquesillo-Lazarte – *Laboratorio de Estudios Cristalográficos, IACT, CSIC-Universidad de Granada, Av. de las Palmeras 4, E-18100 Armilla, Granada, Spain.*

Hongliang Huang – *State Key Laboratory of Separation Membranes and Membrane Processes, School of Chemistry and Chemical Engineering, Tiangong University, Tianjin 300387, China.*

Eduardo Solano – *NCD-SWEET beamline, ALBA Synchrotron Light Source, 08290 Cerdanyola del Vallès, Barcelona, Spain.*

Julio Fraile – *Institut de Ciència de Materials de Barcelona (ICMAB-CSIC) Bellaterra, Spain.*

Clara Viñas – *Institut de Ciència de Materials de Barcelona (ICMAB-CSIC) Bellaterra, Spain.*

Francesc Teixidor – *Institut de Ciència de Materials de Barcelona (ICMAB-CSIC) Bellaterra, Spain.*

Jorge A. R. Navarro – *Departamento de Química Inorgánica, Universidad de Granada, Av. Fuentenueva S/N, E-18071, Granada, Spain.*

Notes

The authors declare no conflict of interest.

ACKNOWLEDGMENTS

L. G., P. G., F. T., C.V. and J.G.P. thank MINECO grant CTQ2016-75150-R and the Generalitat de Catalunya (2017/SGR/1720) for financial support. H. H. thanks the financial support from the National Natural Science Foundation of China (No. 21978212). ICMAB acknowledges the support of the Spanish MINECO through the Severo Ochoa Centers of Excellence Program, under Grant SEV-2015-0496. L. Gan is enrolled in the UAB PhD program. L.G. acknowledges the China

Scholarship Council (CSC) for his PhD grants (201609110106). K.C.S. thanks the Department of Chemistry at Oregon State University for support through the start-up funding. J.A.R.N. thanks MINECO and UE Feder Program (project CTQ2017-84692-R). Some of the experiments were performed at the XALOC and NCD-SWEET beamlines of the ALBA synchrotron with the support of ALBA staff.

REFERENCES

1. V. Masson-Delmotte, P. Z., H. O. Pörtner, D. Roberts, J. Skea, P. R. Shukla, A. Pirani, W. Moufouma-Okia, C. Péan, R. Pidcock, S. Connors, J. B. R. Matthews, Y. Chen, X. Zhou, M. I. Gomis, E. Lonnoy, T. Maycock, M. Tignor, T. Waterfield (eds.), IPCC, 2018: Summary for Policymakers. In: Global warming of 1.5°C. An IPCC Special Report on the impacts of global warming of 1.5°C above pre-industrial levels and related global greenhouse gas emission pathways, in the context of strengthening the global response to the threat of climate change, sustainable development, and efforts to eradicate poverty. *World Meteorological Organization, Geneva, Switzerland, 32 pp.* **2018**.
2. Gough, C., Biomass Energy with Carbon Capture and Storage (BECCS): Unlocking Negative Emissions. *UK: John Wiley & Sons Ltd.* **2018**.
3. Scholz, M.; Hey-Hawkins, E., Carbaboranes as Pharmacophores: Properties, Synthesis, and Application Strategies. *Chem. Rev.* **2011,** *111* (11), 7035-7062.
4. Da Costa, O. M. M. M.; De Azevedo, W. M., Highly luminescent metal organic framework Eu(TMA)(H2O)4 materials prepared by laser ablation technique in liquid. *Journal of Luminescence* **2016,** *170*, 648-653.
5. Lampe, A. I.; Dittmar, A. K.; Heyen, C.; Kiefer, J., Butanol as a potential biofuel: A spectroscopic study of its blends with n-decane and diesel. *Fuel* **2018,** *222*, 312-318.
6. Demirbas, A., Biofuels sources, biofuel policy, biofuel economy and global biofuel projections. *Energy Conversion and Management* **2008,** *49* (8), 2106-2116.
7. Ni, Y.; Sun, Z., Recent progress on industrial fermentative production of acetone–butanol–ethanol by Clostridium acetobutylicum in China. *Applied Microbiology and Biotechnology* **2009,** *83* (3), 415.
8. Xue, C.; Zhao, X.-Q.; Liu, C.-G.; Chen, L.-J.; Bai, F.-W., Prospective and development of butanol as an advanced biofuel. *Biotechnology Advances* **2013,** *31* (8), 1575-1584.
9. Kujawska, A.; Kujawski, J.; Bryjak, M.; Kujawski, W., ABE fermentation products recovery methods—A review. *Renewable and Sustainable Energy Reviews* **2015,** *48*, 648-661.
10. Huang, H.-J.; Ramaswamy, S.; Liu, Y., Separation and purification of biobutanol during bioconversion of biomass. *Separation and Purification Technology* **2014,** *132*, 513-540.
11. Friedl, A., Downstream process options for the ABE fermentation. *FEMS Microbiology Letters* **2016,** *363* (9).
12. Oudshoorn, A.; van der Wielen, L. A. M.; Straathof, A. J. J., Assessment of Options for Selective 1-Butanol Recovery from Aqueous Solution. *Industrial & Engineering Chemistry Research* **2009,** *48* (15), 7325-7336.

13. Abdehagh, N.; Tezel, F. H.; Thibault, J., Adsorbent screening for biobutanol separation by adsorption: kinetics, isotherms and competitive effect of other compounds. *Adsorption* **2013,** *19* (6), 1263-1272.
14. Qureshi, N.; Hp, B., *Recovery of butanol from fermentation broth by gas stripping*. 2018.
15. Abdehagh, N.; Dai, B.; Thibault, J.; Handan Tezel, F., Biobutanol separation from ABE model solutions and fermentation broths using a combined adsorption–gas stripping process. *Journal of Chemical Technology & Biotechnology* **2017,** *92* (1), 245-251.
16. Pyrgakis, K. A.; de Vrije, T.; Budde, M. A. W.; Kyriakou, K.; López-Contreras, A. M.; Kokossis, A. C., A process integration approach for the production of biological iso-propanol, butanol and ethanol using gas stripping and adsorption as recovery methods. *Biochemical Engineering Journal* **2016,** *116*, 176-194.
17. Bhattacharyya, S.; Jayachandrababu, K. C.; Chiang, Y.; Sholl, D. S.; Nair, S., Butanol Separation from Humid CO2-Containing Multicomponent Vapor Mixtures by Zeolitic Imidazolate Frameworks. *ACS Sustainable Chemistry & Engineering* **2017,** *5* (10), 9467-9476.
18. Van der Perre, S.; Gelin, P.; Claessens, B.; Martin-Calvo, A.; Cousin Saint Remi, J.; Duerinck, T.; Baron, G. V.; Palomino, M.; Sánchez, L. Y.; Valencia, S.; Shang, J.; Singh, R.; Webley, P. A.; Rey, F.; Denayer, J. F. M., Intensified Biobutanol Recovery by using Zeolites with Complementary Selectivity. *ChemSusChem* **2017,** *10* (14), 2968-2977.
19. Ding, M.; Flaig, R. W.; Jiang, H.-L.; Yaghi, O. M., Carbon capture and conversion using metal-organic frameworks and MOF-based materials. *Chemical Society Reviews* **2019,** *48* (10), 2783-2828.
20. Trickett, C. A.; Helal, A.; Al-Maythalony, B. A.; Yamani, Z. H.; Cordova, K. E.; Yaghi, O. M., The chemistry of metal-organic frameworks for CO2 capture, regeneration and conversion. *Nature Reviews Materials* **2017,** *2* (8).
21. Furukawa, H.; Cordova, K. E.; O'Keeffe, M.; Yaghi, O. M., The Chemistry and Applications of Metal-Organic Frameworks. *Science* **2013,** *341* (6149), 974-+.
22. Lin, R.-B.; Xiang, S.; Xing, H.; Zhou, W.; Chen, B., Exploration of porous metal–organic frameworks for gas separation and purification. *Coordination Chemistry Reviews* **2019,** *378*, 87-103.
23. Mínguez Espallargas, G.; Coronado, E., Magnetic functionalities in MOFs: from the framework to the pore. *Chemical Society Reviews* **2018,** *47* (2), 533-557.
24. Wang, H.; Zhu, Q.-L.; Zou, R.; Xu, Q., Metal-Organic Frameworks for Energy Applications. *Chem* **2017,** *2* (1), 52-80.
25. Lustig, W. P.; Mukherjee, S.; Rudd, N. D.; Desai, A. V.; Li, J.; Ghosh, S. K., Metal–organic frameworks: functional luminescent and photonic materials for sensing applications. *Chemical Society Reviews* **2017,** *46* (11), 3242-3285.
26. Chen, B.; Eddaoudi, M.; Hyde, S. T.; O'Keeffe, M.; Yaghi, O. M., Interwoven Metal-Organic Framework on a Periodic Minimal Surface with Extra-Large Pores. *Science* **2001,** *291* (5506), 1021-1023.
27. Boyd, P. G.; Chidambaram, A.; García-Díez, E.; Ireland, C. P.; Daff, T. D.; Bounds, R.; Gładysiak, A.; Schouwink, P.; Moosavi, S. M.; Maroto-Valer, M. M.; Reimer, J. A.; Navarro, J. A. R.; Woo, T. K.; Garcia, S.; Stylianou, K. C.; Smit, B., Data-driven design of metal–organic frameworks for wet flue gas CO2 capture. *Nature* **2019,** *576* (7786), 253-256.
28. Ebrahim, F. M.; Nguyen, T. N.; Shyshkanov, S.; Gładysiak, A.; Favre, P.; Zacharia, A.; Itskos, G.; Dyson, P. J.; Stylianou, K. C., Selective, Fast-Response, and Regenerable Metal–

Organic Framework for Sampling Excess Fluoride Levels in Drinking Water. *Journal of the American Chemical Society* **2019,** *141* (7), 3052-3058.
29. Kampouri, S.; Nguyen, T. N.; Spodaryk, M.; Palgrave, R. G.; Züttel, A.; Smit, B.; Stylianou, K. C., Concurrent Photocatalytic Hydrogen Generation and Dye Degradation Using MIL-125-NH2 under Visible Light Irradiation. *Advanced Functional Materials* **2018,** *28* (52), 1806368.
30. Shyshkanov, S.; Nguyen, T. N.; Ebrahim, F. M.; Stylianou, K. C.; Dyson, P. J., In Situ Formation of Frustrated Lewis Pairs in a Water-Tolerant Metal-Organic Framework for the Transformation of CO2. *Angewandte Chemie International Edition* **2019,** *58* (16), 5371-5375.
31. Cousin Saint Remi, J.; Rémy, T.; Van Hunskerken, V.; van de Perre, S.; Duerinck, T.; Maes, M.; De Vos, D.; Gobechiya, E.; Kirschhock, C. E. A.; Baron, G. V.; Denayer, J. F. M., Biobutanol Separation with the Metal–Organic Framework ZIF-8. *ChemSusChem* **2011,** *4* (8), 1074-1077.
32. Zhang, K.; Lively, R. P.; Dose, M. E.; Brown, A. J.; Zhang, C.; Chung, J.; Nair, S.; Koros, W. J.; Chance, R. R., Alcohol and water adsorption in zeolitic imidazolate frameworks. *Chemical Communications* **2013,** *49* (31), 3245-3247.
33. Li, K.; Olson, D. H.; Seidel, J.; Emge, T. J.; Gong, H.; Zeng, H.; Li, J., Zeolitic Imidazolate Frameworks for Kinetic Separation of Propane and Propene. *Journal of the American Chemical Society* **2009,** *131* (30), 10368-10369.
34. Gao, C.; Wu, J.; Shi, Q.; Ying, H.; Dong, J., Adsorption breakthrough behavior of 1-butanol from an ABE model solution with high-silica zeolite: Comparison with zeolitic imidazolate frameworks (ZIF-8). *Microporous and Mesoporous Materials* **2017,** *243*, 119-129.
35. Cousin-Saint-Remi, J.; Denayer, J. F. M., Applying the wave theory to fixed-bed dynamics of Metal-Organic Frameworks exhibiting stepped adsorption isotherms: Water/ethanol separation on ZIF-8. *Chemical Engineering Journal* **2017,** *324*, 313-323.
36. Cousin-Saint-Remi, J.; Finoulst, A.-L.; Jabbour, C.; Baron, G. V.; Denayer, J. F. M., Selection of binder recipes for the formulation of MOFs into resistant pellets for molecular separations by fixed-bed adsorption. *Microporous and Mesoporous Materials* **2019**, 109322.
37. Cousin-Saint-Remi, J.; Van der Perre, S.; Segato, T.; Delplancke, M.-P.; Goderis, S.; Terryn, H.; Baron, G.; Denayer, J., Highly Robust MOF Polymeric Beads with a Controllable Size for Molecular Separations. *ACS Applied Materials & Interfaces* **2019,** *11* (14), 13694-13703.
38. Liu, X.; He, L.; Zheng, J.; Guo, J.; Bi, F.; Ma, X.; Zhao, K.; Liu, Y.; Song, R.; Tang, Z., Solar-Light-Driven Renewable Butanol Separation by Core–Shell Ag@ZIF-8 Nanowires. *Advanced Materials* **2015,** *27* (21), 3273-3277.
39. Liu, X.-L.; Li, Y.-S.; Zhu, G.-Q.; Ban, Y.-J.; Xu, L.-Y.; Yang, W.-S., An Organophilic Pervaporation Membrane Derived from Metal–Organic Framework Nanoparticles for Efficient Recovery of Bio-Alcohols. *Angewandte Chemie International Edition* **2011,** *50* (45), 10636-10639.
40. Bai, Y.; Dong, L.; Zhang, C.; Gu, J.; Sun, Y.; Zhang, L.; Chen, H., ZIF-8 Filled Polydimethylsiloxane Membranes for Pervaporative Separation of n-Butanol from Aqueous Solution. *Separation Science and Technology* **2013,** *48* (17), 2531-2539.
41. Li, Y.; Wee, L. H.; Martens, J. A.; Vankelecom, I. F. J., ZIF-71 as a potential filler to prepare pervaporation membranes for bio-alcohol recovery. *Journal of Materials Chemistry A* **2014,** *2* (26), 10034-10040.
42. Tan, F.; López-Periago, A.; Light, M. E.; Cirera, J.; Ruiz, E.; Borrás, A.; Teixidor, F.; Viñas, C.; Domingo, C.; Planas, J. G., An Unprecedented Stimuli-Controlled Single-Crystal

Reversible Phase Transition of a Metal–Organic Framework and Its Application to a Novel Method of Guest Encapsulation. *Adv. Mater.* **2018,** *30* (29), 1800726.
43. Tsang, M. Y.; Rodríguez-Hermida, S.; Stylianou, K. C.; Tan, F.; Negi, D.; Teixidor, F.; Viñas, C.; Choquesillo-Lazarte, D.; Verdugo-Escamilla, C.; Guerrero, M.; Sort, J.; Juanhuix, J.; Maspoch, D.; Giner Planas, J., Carborane Bis-pyridylalcohols as Linkers for Coordination Polymers: Synthesis, Crystal Structures, and Guest-Framework Dependent Mechanical Properties. *Crystal Growth & Design* **2017,** *17* (2), 846-857.
44. Rodriguez-Hermida, S.; Tsang, M. Y.; Vignatti, C.; Stylianou, K. C.; Guillerm, V.; Perez-Carvajal, J.; Teixidor, F.; Vinas, C.; Choquesillo-Lazarte, D.; Verdugo-Escamilla, C.; Peral, I.; Juanhuix, J.; Verdaguer, A.; Imaz, I.; Maspoch, D.; Giner Planas, J., Switchable Surface Hydrophobicity-Hydrophilicity of a Metal-Organic Framework. *Angew Chem Int Ed Engl* **2016,** *55* (52), 16049-16053.
45. Grimes, R. N., Carboranes. In *Carboranes (Third Edition)*, Academic Press: Oxford, 2016.
46. Teixidor, F.; Viñas, C., In *Science of Synthesis*, D.E., K.; D.S., M., Eds. Thieme: Stuttgart, 2005; Vol. 6, pp 1325-1275.
47. Fujii, S., Expanding the chemical space of hydrophobic pharmacophores: the role of hydrophobic substructures in the development of novel transcription modulators. *MedChemComm* **2016,** *7* (6), 1082-1092.
48. Fontanet, M.; Popescu, A.-R.; Fontrodona, X.; Rodríguez, M.; Romero, I.; Teixidor, F.; Viñas, C.; Aliaga-Alcalde, N.; Ruiz, E., Design of Dinuclear Copper Species with Carboranylcarboxylate Ligands: Study of Their Steric and Electronic Effects. *Chemistry – A European Journal* **2011,** *17* (47), 13217-13229.
49. Teixidor, F.; Barberà, G.; Vaca, A.; Kivekäs, R.; Sillanpää, R.; Oliva, J.; Viñas, C., Are methyl groups electron-donating or electron-withdrawing in boron clusters? Permethylation of o-carborane. *Journal of the American Chemical Society* **2005,** *127* (29), 10158-10159.
50. Poater, J.; Solà, M.; Viñas, C.; Teixidor, F., π Aromaticity and Three-Dimensional Aromaticity: Two sides of the Same Coin. *Angewandte Chemie - International Edition* **2014,** *53* (45), 12191-12195.
51. Nakamura, H.; Aoyagi, K.; Yamamoto, Y., o-Carborane as a Novel Protective Group for Aldehydes and Ketones. *Journal of Organic Chemistry* **1997,** *62* (4), 780-781.
52. Núñez, R.; Romero, I.; Teixidor, F.; Viñas, C., Icosahedral boron clusters: a perfect tool for the enhancement of polymer features. *Chemical Society Reviews* **2016,** *45* (19), 5147-5173.
53. Issa, F.; Kassiou, M.; Rendina, L. M., Boron in Drug Discovery: Carboranes as Unique Pharmacophores in Biologically Active Compounds. *Chem. Rev.* **2011,** *111* (9), 5701-5722.
54. In *Boron-Based Compounds. Potential and Emerging applications in Medicine*, Teixidor, E. H.-H. a. C. V., Ed. John Wiley & Sons Ltd: UK, 2018.
55. Clara, V.; Rosario, N.; Ines, B.; Francesc, T., Periphery Decorated and Core Initiated Neutral and Polyanionic Borane Large Molecules: Forthcoming and Promising Properties for Medicinal Applications. *Current Medicinal Chemistry* **2019,** *26* (26), 5036-5076.
56. Hosmane, N., In *Boron Science*, CRC Press: **Boca Raton**, 2012.
57. *Handbook of Boron Chemistry in Organometallics, Catalysis, Materials and Medicine*. mperial College Press/World Scientific Publishing Ltd.: UK, 2018; p 1400.
58. Gan, L.; Fonquernie, P. G.; Light, M. E.; Norjmaa, G.; Ujaque, G.; Choquesillo-Lazarte, D.; Fraile, J.; Teixidor, F.; Viñas, C.; Planas, J. G., A Reversible Phase Transition of 2D Coordination Layers by B–H···Cu(II) Interactions in a Coordination Polymer. *Molecules* **2019,** *24* (17), 3204.

59. Chung, H.; Barron, P. M.; Novotny, R. W.; Son, H.-T.; Hu, C.; Choe, W., Structural Variation in Porphyrin Pillared Homologous Series: Influence of Distinct Coordination Centers for Pillars on Framework Topology. *Cryst. Growth Des.* **2009,** *9* (7), 3327-3332.
60. Jiang, H.-L.; Makal, T. A.; Zhou, H.-C., Interpenetration control in metal–organic frameworks for functional applications. *Coord. Chem. Rev.* **2013,** *257* (15), 2232-2249.
61. Zhan, C.-H.; Feng, Y.-L., A novel 44.66 5-connected metal-organic framework with strong fluorescent emission constructed by m-thioacetatebenzoic acid. *Journal of Solid State Chemistry* **2010,** *183* (6), 1226-1230.
62. Wang, J.; Wu, X.-R.; Liu, J.-Q.; Li, B.-H.; Singh, A.; Kumar, A.; Batten, S. R., An uncommon (5,5)-connected 3D metal organic material for selective and sensitive sensing of nitroaromatics and ferric ion: experimental studies and theoretical analysis. *CrystEngComm* **2017,** *19* (25), 3519-3525.
63. Eubank, J. F.; Wojtas, L.; Hight, M. R.; Bousquet, T.; Kravtsov, V. C.; Eddaoudi, M., The Next Chapter in MOF Pillaring Strategies: Trigonal Heterofunctional Ligands To Access Targeted High-Connected Three Dimensional Nets, Isoreticular Platforms. *J. Am. Chem. Soc.* **2011,** *133* (44), 17532-17535.
64. Wang, H.-N.; Meng, X.; Yang, G.-S.; Wang, X.-L.; Shao, K.-Z.; Su, Z.-M.; Wang, C.-G., Stepwise assembly of metal–organic framework based on a metal–organic polyhedron precursor for drug delivery. *Chem. Commun.* **2011,** *47* (25), 7128-7130.
65. Klein, N.; Senkovska, I.; Baburin, I. A.; Grünker, R.; Stoeck, U.; Schlichtenmayer, M.; Streppel, B.; Mueller, U.; Leoni, S.; Hirscher, M.; Kaskel, S., Route to a Family of Robust, Non-interpenetrated Metal–Organic Frameworks with pto-like Topology. *Chem. Eur. J.* **2011,** *17* (46), 13007-13016.
66. Müller, P.; Wisser, F. M.; Freund, P.; Bon, V.; Senkovska, I.; Kaskel, S., Optical Sensors Using Solvatochromic Metal–Organic Frameworks. *Inorg. Chem.* **2017,** *56* (22), 14164-14169.
67. Jasuja, H.; Walton, K. S., Effect of catenation and basicity of pillared ligands on the water stability of MOFs. *Dalton Trans.* **2013,** *42* (43), 15421-15426.
68. Park, S. S.; Hendon, C. H.; Fielding, A. J.; Walsh, A.; O'Keeffe, M.; Dincă, M., The Organic Secondary Building Unit: Strong Intermolecular π Interactions Define Topology in MIT-25, a Mesoporous MOF with Proton-Replete Channels. *J. Am. Chem. Soc.* **2017,** *139* (10), 3619-3622.
69. Gelfand, B. S.; Shimizu, G. K. H., Parameterizing and grading hydrolytic stability in metal–organic frameworks. *Dalton Trans.* **2016,** *45* (9), 3668-3678.
70. Shtukenberg, A. G.; Punin, Y. O.; Gunn, E.; Kahr, B., Spherulites. *Chem. Rev.* **2012,** *112* (3), 1805-1838.
71. DeCoste, J. B.; Peterson, G. W.; Schindler, B. J.; Killops, K. L.; Browe, M. A.; Mahle, J. J., The effect of water adsorption on the structure of the carboxylate containing metal–organic frameworks Cu-BTC, Mg-MOF-74, and UiO-66. *J. Mater. Chem. A* **2013,** *1* (38), 11922-11932.
72. He, H.; Sun, Q.; Gao, W.; Perman, J. A.; Sun, F.; Zhu, G.; Aguila, B.; Forrest, K.; Space, B.; Ma, S., A Stable Metal–Organic Framework Featuring a Local Buffer Environment for Carbon Dioxide Fixation. *Angew. Chem. Int. Ed.* **2018,** *57* (17), 4657-4662.
73. Canivet, J.; Fateeva, A.; Guo, Y.; Coasne, B.; Farrusseng, D., Water adsorption in MOFs: fundamentals and applications. *Chem. Soc. Rev.* **2014,** *43* (16), 5594-5617.
74. PXRD experiments confirmed the stability of the MOF after being shaped into a pellet.
75. Sann, E. E.; Pan, Y.; Gao, Z.; Zhan, S.; Xia, F., Highly hydrophobic ZIF-8 particles and application for oil-water separation. *Separation and Purification Technology* **2018,** *206*, 186-191.

76. Jayaramulu, K.; Geyer, F.; Schneemann, A.; Kment, S.; Otyepka, M.; Zboril, R.; Vollmer, D.; Fischer, R. A., Hydrophobic Metal-Organic Frameworks. *Adv Mater* **2019,** *31* (32), e1900820.
77. Myers, A. L.; Prausnitz, J. M., Thermodynamics of mixed-gas adsorption. *AIChE Journal* **1965,** *11* (1), 121-127.
78. Fox, M. A., Icosahedral carborane derivatives. *Durham theses, Durham University.* **1991**.
79. Juanhuix, J.; Gil-Ortiz, F.; Cuni, G.; Colldelram, C.; Nicolas, J.; Lidon, J.; Boter, E.; Ruget, C.; Ferrer, S.; Benach, J., Developments in optics and performance at BL13-XALOC, the macromolecular crystallography beamline at the Alba Synchrotron. *Journal of Synchrotron Radiation* **2014,** *21* (4), 679-689.
80. Dolomanov, O. V.; Bourhis, L. J.; Gildea, R. J.; Howard, J. A. K.; Puschmann, H., OLEX2: a complete structure solution, refinement and analysis program. *Journal of Applied Crystallography* **2009,** *42* (2), 339-341.
81. Sheldrick, G., Crystal structure refinement with SHELXL. *Acta Crystallographica Section C* **2015,** *71* (1), 3-8.
82. Kieffer, J.; Karkoulis, D., PyFAI, a versatile library for azimuthal regrouping. *Journal of Physics: Conference Series* **2013,** *425* (20), 202012.
83. Babarao, R.; Hu, Z.; Jiang, J.; Chempath, S.; Sandler, S. I., Storage and Separation of CO2 and CH4 in Silicalite, C168 Schwarzite, and IRMOF-1: A Comparative Study from Monte Carlo Simulation. *Langmuir* **2007,** *23* (2), 659-666.
84. Goetz, V.; Pupier, O.; Guillot, A., Carbon dioxide-methane mixture adsorption on activated carbon. *Adsorption* **2006,** *12* (1), 55-63.
85. Biovia Materials Studio 6.0: San Diego: Dassault Systèmes 2018.
86. Sun, H., COMPASS: An ab Initio Force-Field Optimized for Condensed-Phase ApplicationsOverview with Details on Alkane and Benzene Compounds. *The Journal of Physical Chemistry B* **1998,** *102* (38), 7338-7364.
87. Vandevondele, J.; Krack, M.; Mohamed, F.; Parrinello, M.; Chassaing, T.; Hutter, J., Quickstep: Fast and accurate density functional calculations using a mixed Gaussian and plane waves approach. *Computer Physics Communications* **2005,** *167* (2), 103-128.
88. Goedecker, S.; Teter, M., Separable dual-space Gaussian pseudopotentials. *Physical Review B - Condensed Matter and Materials Physics* **1996,** *54* (3), 1703-1710.
89. Hartwigsen, C.; Goedecker, S.; Hutter, J., Relativistic separable dual-space Gaussian pseudopotentials from H to Rn. *Physical Review B - Condensed Matter and Materials Physics* **1998,** *58* (7), 3641-3662.
90. Krack, M.; Parrinello, M., All-electron ab-initio molecular dynamics. *Physical Chemistry Chemical Physics* **2000,** *2* (10), 2105-2112.
91. VandeVondele, J.; Hutter, J., Gaussian basis sets for accurate calculations on molecular systems in gas and condensed phases. *The Journal of Chemical Physics* **2007,** *127* (11), 114105.
92. Perdew, J. P.; Burke, K.; Ernzerhof, M., Generalized gradient approximation made simple (vol 77, pg 3865, 1996). *Physical Review Letters* **1997,** *78* (7), 1396-1396.
93. Grimme, S.; Antony, J.; Ehrlich, S.; Krieg, H., A consistent and accurate ab initio parametrization of density functional dispersion correction (DFT-D) for the 94 elements H-Pu. *Journal of Chemical Physics* **2010,** *132* (15).

For Table of Contents Only